19th Brazilian Congress of Thermal Sciences and Engineering
November 6th–10th, 2022, Bento Gonçalves - RS - Brazil

ENC-2022-0383
A NUMERICAL INVESTIGATION ON CONCENTRATED EMULSIONS IN SIMPLE SHEAR FLOW

Raysa Gomes dos Santos
Taygoara Felamingo de Oliveira
Department of Mechanical Engineering, University of Brasília, Brasília, DF 70910-900, Brazil
raysagoms@gmail.com; taygoara@unb.br

Abstract. *This work explores the effects of droplet interactions in a concentrated emulsion under a simple shear flow. Our analysis considers a two-dimensional numerical domain where monodisperse Newtonian droplets flow under simple shear conditions in a Newtonian ambient fluid. The surface of the droplets is assumed to be free of surfactants, and we consider both phases with the same density and viscosity. The numerical methodology uses the projection method for pressure-velocity coupling and the Crank-Nicolson method for the temporal evolution of the momentum equation. Spatial discretization is carried out using second-order discretization and the staggered grids. The level set method is used for tracking the interfaces of the droplets. High order essentially nonoscillatory (ENO) and weighted essentially nonoscillatory (WENO) conservative schemes, with a total variation diminishing (TVD) Runge-Kutta method, are used to discretize the level set equations. A method for generation of the initial position of the droplets, capable of setting up an emulsion of a given concentration, with droplets randomly spread in the ambient fluid is proposed. We study the flow for different droplet concentrations and capillary numbers. We found that, at low capillary numbers, the coalescence process increases as the volume fraction of the dispersed phase increases. On the other hand, for high capillary numbers, droplet merging decreases for any concentration in the range adopted in this investigation. They tend to slide over each other due to the decreased interfacial tension. In both cases, however, our results indicate that the coalescence rate could be higher than expected for the flow conditions, indicating that it is necessary to implement methods to avoid artificial droplet merging.*

Keywords: *concentrated emulsions, level set method, coalescence, finite difference*

1. INTRODUCTION

Emulsions are complex fluids composed of a dispersed phase (droplets) suspended in an immiscible liquid (continuous phase). In the absence of surfactants, these systems are quite unstable, and therefore mechanisms such as sedimentation, coalescence, flocculation, and Ostwald ripening are more likely to happen. Understanding the conditions under which these destabilization processes occur has an essential role in the industry due to its advantages. In the oil industry, the processing of crude oil often requires the extraction of water, and one of the demulsification techniques is done by using electrocoalescence (Eow *et al.*, 2001). In microfluidic technology, there are many strategies to destabilize emulsion droplets because they have a highly monodisperse size distribution which allows us to induce destabilization in a controlled manner. Applications can be found in biological flows (e.g., drug delivery systems, and tissue engineering) (Santos *et al.*, 2022; Li *et al.*, 2018), and in the pharmaceutical science and technology to lower costs and reagent consumption (Cui and Wang, 2019).

The behavior of emulsions depends on the concentration of the dispersed phase, which can be specificated as diluted, moderated, and concentrated. The variable to express the effect of concentration in these systems is the droplet volume fraction (ϕ). Overall, most emulsions of daily life have a high volume fraction, however, the dynamic of a single droplet has been extensively studied. Previous experimental studies investigated the deformation and breakup of suspensions of rigid and deformable particles in a diluted context; thus, the droplets interactions are neglected. Taylor (1934) and Grace (1982) found that for each viscosity ratio between the dispersed and continuous phases there is a critical capillary number that the drop breaks, and there is a limit, in which the droplet, at low capillary numbers, cannot breakup in shear flow. Moreover, they analyzed the orientation angle and the deformation of the drop concerning the flow direction and realized that inertial forces did not affect the shape of the drop. In the case of highly deformed droplets, Vananroye *et al.* (2006) showed that when the particles are greatly confined, breakup with high viscosity ratios in a simple shear flow field

becomes possible, Guido (2011) identified it numerically based on the boundary-integral formulation. Kennedy *et al.* (1994) performed a numerical analysis of the deformation of a single drop using the boundary-integral method for Stokes flow, and also identified that even in dilute cases the emulsions exhibit elastic behavior for all values of the viscosity ratio, $\lambda = \mu_d/\mu_d$ where μ is the dynamic viscosity, and subscript d and c indicate the dispersed phase and continuum phase, in that order.

In contrast to dilute cases, the behavior of droplets in concentrated emulsions becomes a more complex problem because the interaction with surrounding droplets is significant. In this context, Jansen *et al.* (2001) studied experimentally the conditions for droplet breakage under simple shear. These authors showed that the critical capillary number for breakage decreased in concentrated emulsions. Loewenberg and Hinch (1996) were one of the first in numerical simulations of deformable particles in a concentrated regime. They used the boundary integral method to simulate droplet collisions in shear flow. From their results, it follows that the effect of concentration on breakup is relatively small for $\phi \leq 30\%$, and the resulting anisotropic self-diffusivities are strongly dependent on viscosity ratio. In addition, Rosti *et al.* (2019) studied the dependency of the effective viscosity on the volume fraction and the capillary number Ca when the drops can merge. They found out that at a fixed Ca and increasing ϕ, the total surface area reduces due to the merging.

Coalescence is an important process that is related to attractive and repulsive interactions, volume fraction, and droplet size. This process happens when there is a thinning and disruption of the liquid film between the droplets during a collision, and they fuse into larger ones reducing the total surface area until the complete separation of the liquids phases (Tadros, 2016). Furthermore, to prevent film rupture the repulsive forces play an important role, especially in concentrated emulsions, since the coalescence rate increases with increasing concentration, which leads to changes in the droplet size distribution and, consequently, changes in macroscopic properties (Sundararaj and Macosko, 1995). Chen *et al.* (2009) studied experimentally the effect of confinement on coalescence. These authors reported that both the coalescence angle and the critical number are influenced by the presence of the walls. In addition, they pointed out that generally occur three consecutive steps in this process: approach, drainage, and rupture of the liquid film. Chen and Wang (2014) used the volume-of-fluid (VOF) method to represent the free interface behaviors involved in two interactive drops. They found two types of drop behaviors during interaction occur including passing-over motion and reversing motion. In the VOF and level set methods, two drops merge when the chosen grid size cannot resolve the gap between them; thus, having a high resolution on the grid is of paramount importance, while taking a long time is needed for the film to drain before rupturing (Shardt *et al.*, 2013). De Vita *et al.* (2019) with VOF simulated the coalescence process in concentrated emulsions using a short-range repulsive interactions model.

In this work, we investigate the dynamic of monodisperse droplets spread randomly under simple shear from a macroscopic point of view. A two-dimensional domain (2D) with periodic boundary conditions is imposed. The numerical methods include the level set technique to capture the droplets' interfaces and the projection method to solve the hydrodynamic problem. We simulated this system for different values of volume fraction and capillary numbers. The viscosity and density of both phases are assumed to be the same, and the Reynolds number is low enough for inertial forces to be negligible. Our results indicate that, at a fixed capillary number, as the volume fraction of the dispersed phase increases the merging rate of the droplets increases more than expected, indicating that it is necessary to implement methods to avoid artificial droplet merging.

2. NUMERICAL MODEL

The schematic channel where the droplets are placed is shown in Fig. 1. We consider the analyses of a monodisperse suspension of deformable liquid drops suspended in an ambient fluid with the same viscosity and density, $\lambda = 1$ and $\rho = 1$ in all simulations, we further do not consider the gravity effect. Furthermore, both phases are incompressible Newtonian. At the initial time, the shape of the drops is circular with a unit diameter d, and they are located in random positions in the channel with $L_x \times L_y$ domain with non-overlap condition. It has two horizontal parallel plates that moves in opposite directions with same velocity U whith causes a shear flow of shear rate $\dot{\gamma}$. A periodic flow condition is implemented in the x-direction at the left and right wall of the flow domain. The most important nondimensional parameters that affect emulsion rheology in this work are as follows:

$$Re = \frac{\rho_c \dot{\gamma} d^2}{\mu_c}, \tag{1}$$

$$Ca = \frac{\mu_c d \dot{\gamma}}{\sigma}, \tag{2}$$

and

$$\phi = \frac{N A_d}{A_c}, \tag{3}$$

where Re denotes the Reynolds number which indicates the relative importance between the advective term and the viscous term, here, ρ_c and μ_c are the density and the viscosity of continuous phase, respectively. The effects of surface

tension σ are captured by the capillary number Ca, which represents the ratio between viscous forces and capillary forces. Finally, ϕ is volume fraction of the dispersed phase where N is the number of drops, A_d is the area of each drop and A_d is the area occupied by the base fluid.

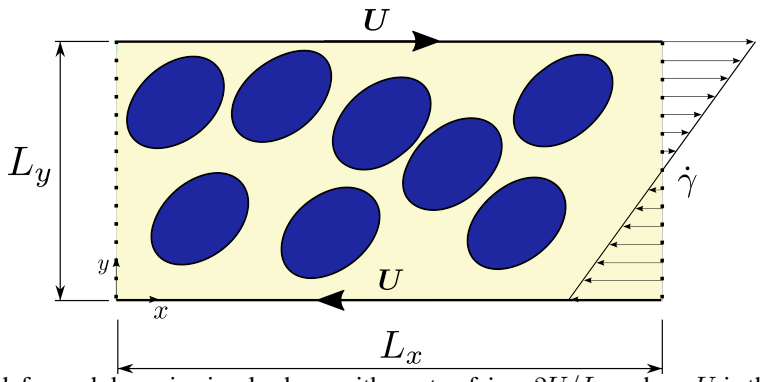

Figure 1: schematics of deformed drops in simple shear with a rate of $\dot{\gamma} = 2U/L_y$, where U is the velocity of the top and bottom walls that moving in opposite directions. The periodic boundary condition is imposed on the two vertical walls. The definitions of the coordinate axes and its dimension are shown.

3. NUMERICAL DESCRIPTION

3.1 Level set method

To capture the liquid-liquid interface of two-phase flow, we used the level set method proposed by Osher and Sethian (1988). This method defines the interface as the zero value of a distance function $\varphi(\mathbf{x}, t)$, which has a positive value for the inner fluid region and a negative value for the outer fluid region. In short, at each instant of time, the surface of the drop is determined by a set of points that satisfy the function $\varphi(\mathbf{x}, t) = 0$. In a continuum formulation, the interface is always composed of the same φ points, so it is treated as a property that is conserved over time. Hence, the level set function moves with the velocity of fluid $\boldsymbol{u}$ through the following equation:

$$\frac{\partial \varphi}{\partial t} + \boldsymbol{u} \cdot \nabla \varphi = 0. \tag{4}$$

Note that $\nabla\varphi$ is orthogonal to the interface which allows us to define the normal vector and therefore the curvature of the interface, respectively, as

$$\hat{\boldsymbol{n}} = \frac{\nabla \varphi}{|\nabla \varphi|}, \text{ and } \kappa = \nabla \cdot \hat{\boldsymbol{n}}. \tag{5}$$

The function φ can be also used to define properties that are different outside and inside the drops, so due to the discontinuity that exists through the interface owing to these differences in properties, a modified Heaviside function is used to smoothes this jump

$$H(\varphi) = \begin{cases} 0, & \text{if } \varphi < -\epsilon \\ \dfrac{1}{2}\left[1 + \dfrac{\varphi}{\epsilon} + \dfrac{1}{\pi}\sin\left(\dfrac{\pi\varphi}{\epsilon}\right)\right], & \text{if } -\epsilon \leq \varphi \leq \epsilon \\ 1, & \text{if } \epsilon < \varphi, \end{cases} \tag{6}$$

where ϵ represents the thickness of the interface, in this work it is given by $1.5\Delta x$, where Δx is the size of a grid cell. From this, we can set the smoothed delta Dirac function as

$$\delta(\varphi) = \frac{\partial H(\varphi)}{\partial \varphi} = \begin{cases} 0, & \text{if } \varphi < -\epsilon \\ \dfrac{1}{2\epsilon}\left[1 + \cos\left(\dfrac{\pi\varphi}{\epsilon}\right)\right], & \text{if } -\epsilon \leq \varphi \leq \epsilon \\ 0, & \text{if } \epsilon < \varphi. \end{cases} \tag{7}$$

Finally, the Eq. (4) is solved with a combined third-order TVD Runge-Kutta method for the temporal discretization and a fifth-order Weighted Essentially Non-Oscillator (WENO) scheme for the computation of the spatial derivative. To ensure that $\varphi(\mathbf{x}, t)$ can remain as a distance function and to conserve mass bounded by the interface, a re-initialization equation is solved in three iterations per time step as made by Sussman *et al.* (1994). In other words, this step ensures that the condition $|\nabla\varphi| = 1$ is satisfied, and the normal vector and the curvature of the interface are preserved as unit vectors, which allows us to define the interface correctly.

3.2 Governing equations

The movement equations governing the two-phase flow in our context are the continuity and Navier-Stokes coupled with capillary forces, respectively given by

$$\nabla \cdot \boldsymbol{u} = 0, \tag{8}$$

and

$$\rho \frac{D\boldsymbol{u}}{Dt} = -\nabla p + \nabla \cdot (2\mu \boldsymbol{D}) + \boldsymbol{F}_\sigma. \tag{9}$$

Here, $\boldsymbol{u}$ is velocity field, p is pressure, $D/Dt = \partial/\partial t + \boldsymbol{u} \cdot \nabla$ is the material derivative, $\boldsymbol{D} = 1/2[\nabla \boldsymbol{u} + (\nabla \boldsymbol{u})^T]$ is the strain rate tensor, μ is the viscosity, and ρ is the density. In addition, the term $\boldsymbol{F}_\sigma$ denotes the continuum body force due to interfacial tension,

$$\boldsymbol{F}_\sigma = -\sigma \kappa \delta(\varphi) \hat{\boldsymbol{n}}, \tag{10}$$

where σ is the surface tension coefficient, κ the local mean curvature, $\hat{\boldsymbol{n}}$ denotes the unit normal outwards from the interface, and $\delta(\varphi)$ is the Dirac delta function applied to the level set function. Substituting Eq. (10) in Eq. (9) and using the following parameters:

$$\tilde{\boldsymbol{u}} = \frac{\boldsymbol{u}}{\dot{\gamma} d}, \quad \tilde{t} = t\dot{\gamma}, \quad \tilde{p} = \frac{p}{\rho d^2 \dot{\gamma}^2}, \quad \tilde{\nabla} = d\nabla,$$

the governing Eqs. (8) and (9) can be written as:

$$\tilde{\nabla} \cdot \tilde{\boldsymbol{u}} = 0, \tag{11}$$

$$\frac{\partial \tilde{\boldsymbol{u}}}{\partial \tilde{t}} + \tilde{\boldsymbol{u}} \cdot \tilde{\nabla} \tilde{\boldsymbol{u}} = -\tilde{\nabla} \tilde{p} + \frac{1}{Re} \tilde{\nabla}^2 \tilde{\boldsymbol{u}} - \frac{1}{CaRe} \tilde{\boldsymbol{F}}_\sigma. \tag{12}$$

Dimensionless groups are explained in Section 2. Hereafter we omit the tilde from these equations.

3.3 Projection method

The hydrodynamic problem that governs the velocity and pressure fields is solved using the modified second-order projection method. For this, the discretization of the 2D domain is done by a uniform rectangular cartesian staggered grid, i.e., fluid velocities are located on the cell faces, and all other variables are located at the cell centers, while second-order finite differences are used to discretize the problem domain. Therefore, Eqs. (11) and (12) are solved as

$$\frac{\boldsymbol{u}^* - \boldsymbol{u}^n}{\Delta t} = -(\boldsymbol{u} \cdot \nabla \boldsymbol{u})^{n+1/2} + \frac{1}{2Re} \nabla^2 (\boldsymbol{u}^* + \boldsymbol{u}^n) - \frac{1}{ReCa} \left[\delta(\varphi) \kappa \boldsymbol{n}\right]^{n+1/2}, \tag{13}$$

and

$$\frac{\boldsymbol{u}^{n+1} - \boldsymbol{u}^*}{\Delta t} = -(\nabla \chi)^{n+1}, \tag{14}$$

here, $\boldsymbol{u}^*$ is a tentative velocity field, and χ is an auxiliary pressure. All terms are temporally computed at $t + 1/2$ as Crank–Nicolson scheme to obtain a complete second order method. Advective terms are extrapolated by the Adam-Bashforth method and is solved by the second order essentially non-oscillatory (ENO) scheme with upwind. To obtain an adequate equation for χ, we take the divergence of Eq. (14),

$$\frac{\nabla \cdot \boldsymbol{u}^*}{\Delta t} = \nabla^2 \chi^{n+1} \tag{15}$$

Thus, the pressure and velocity fields at $n + 1$ are computed by

$$\boldsymbol{u}^{n+1} = \boldsymbol{u}^* - \Delta t \nabla \chi^{n+1}, \tag{16}$$

and

$$p^{n+1} = \chi^{n+1} - \frac{\Delta t}{2Re\tilde{\rho}(\phi)} \nabla \cdot \boldsymbol{u}^*. \tag{17}$$

4. RESULTS AND DISCUSSION

4.1 Single drop shape

At first, we simulate a single droplet in a simple shear and compare it to those in the literature in terms of deformation D and the orientation angle θ, to certify whether our numerical model has a good agreement. We use a domain size of 12×6 discretized with a uniform staggered grid with 256×128 cells. It was fixed the parameters $Re = 0.01$ and $d = 1$. Ioannou *et al.* (2016) pointed out that the wall effect can be negligible to droplet deformation for the confinement ratio $d/L_y < 0.4$ at $\lambda = 1$, in this work we use $d/L_y \approx 0.17$. We set the time step in $\Delta t = 2.5 \times 10^{-4}$ and simulate until steady state. The deformation parameter of a droplet suspended in another viscous fluid under a simple shear at Stokes flow can be defined as $D = (L - B)/(L + B)$, where L and B are the dimensions of the major and minor axes of the ellipse formed by the deformed drop, respectively. In the limit where $L = B$ we have that the deformation is zero, that is, the drop remains circular. In Fig. 2 (right) the orientation angle of the drop is formed between the principal axis of the drop and the direction of flow. Since there is a greater deformation of the drop to a larger capillary numbers, the orientation angle of the drop respectively decreases as Ca increases, as it tends to align with the flow. In addition, the comparison with the numerical results of Guido (2011) and Kennedy *et al.* (1994) shows very good agreement with each other, as well as the theoretical results of Taylor (1934) in terms of the deformation of the droplet.

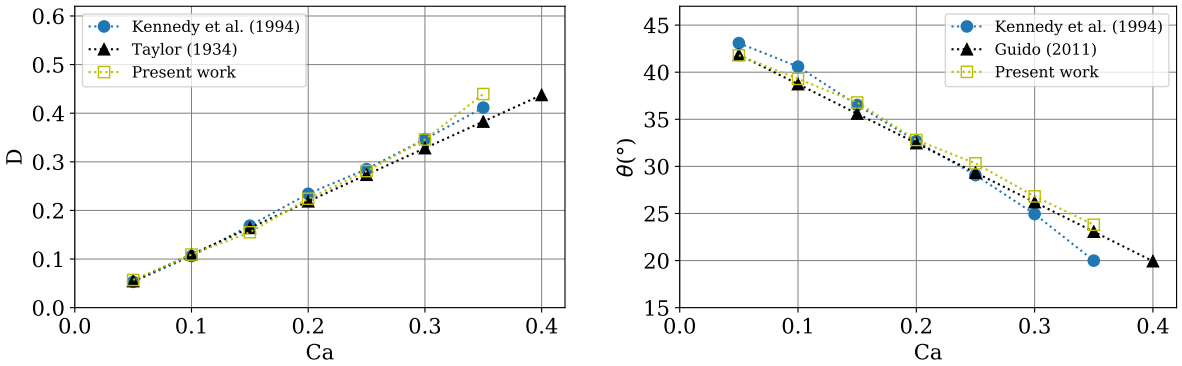

Figure 2: droplet deformation as a function of the capillary number compared with the numerical simulation of Kennedy *et al.* (1994) and Taylor's theory (Taylor, 1934) (left). Comparison of orientation angle with simulation results of Kennedy *et al.* (1994) and Guido (2011) at $\lambda = 1$ (right).

4.2 Droplets in simple shear with different concentrations and capillary number

In this subsection, we discuss our analysis of the change in concentration of monodisperse droplets under simple shear. First, we set three capillary numbers $Ca = \{0.05, 0.20, 0.35\}$ and simulated them for different volume fractions of the dispersed phase, $\phi = \{0.1, 0.2, 0.35\}$. All simulations are conducted at $Re = 0.1$ and $d = 1$. Both fluids are assumed to have equal densities and viscosity. We use a domain size of 12×6 discretized with a uniform staggered grid with 256×128 cells, then all the results presented in this study are grid independent and with negligible wall effect. Moreover, a periodic boundary condition is implemented in the two y-direction vertical walls.

As noted earlier, the process of coalescence occurs when thinning of the interfacial film results in rupture, *i.e.*, the droplets tend to approach each other and irreversibly coalesce, forming larger droplets until it again becomes a continuous phase separated from the dispersed phase, as a consequence of van der Waals attraction (Tadros, 2016). Although numerical schemes like the level set might be a good choice for simulating complex geometries, including the merging process, they are not able to predict phenomena that happen at the microscale. Droplet breakup and coalescence predicted by the standard LS method results from the macroscopic hydrodynamics combined with the transport and reinitialization of the ϕ. The delicate mechanisms responsible for the interface topological transitions are absent in the formulation, and their inclusion is one of the long-term goals of this work.

Figure 3a shows the first iteration with $\phi = 10\%$ for randomly spread drops, Fig. 3b has the same configuration but at time $t = 100$. From these plots, it can be seen that the closest arranged drops merged into one, even with high interfacial tension. Note that there was not much deformation in the shape of the drops. Figures 3c and 3d were plotted at the same time as the previous ones, but with a volume fraction of the dispersed phase of $\phi = 20\%$. In this case, there are much more drops next to each other and, consequently, more mergers occur. In fact, some drops at the final instant are larger in size compared to the previous case of smaller volume fraction. The last row in Fig. 3 corresponds to the case with $\phi = 35\%$, here, more drops coalesce and form others with sizes larger than the last case. Although it seems that the drops deform more, this is not true as we do not set another Ca, the droplets are just in the process of merging.

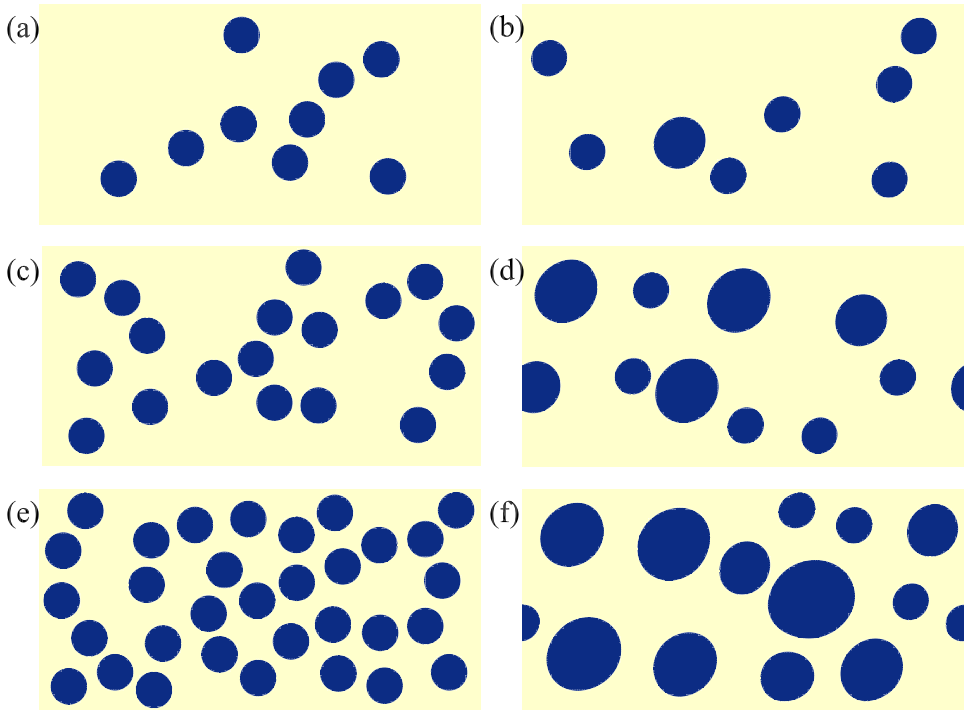

Figure 3: droplets spread randomly at fixed capillary number $Ca = 0.05$. Time progress from $t = 0$ (column left) to $t = 100$ (column right). Three volume fraction was considered, increasing from top to bottom. The portion (a-b) $\phi = 10\%$; (c-d) $\phi = 20\%$; (e-f) $\phi = 35\%$.

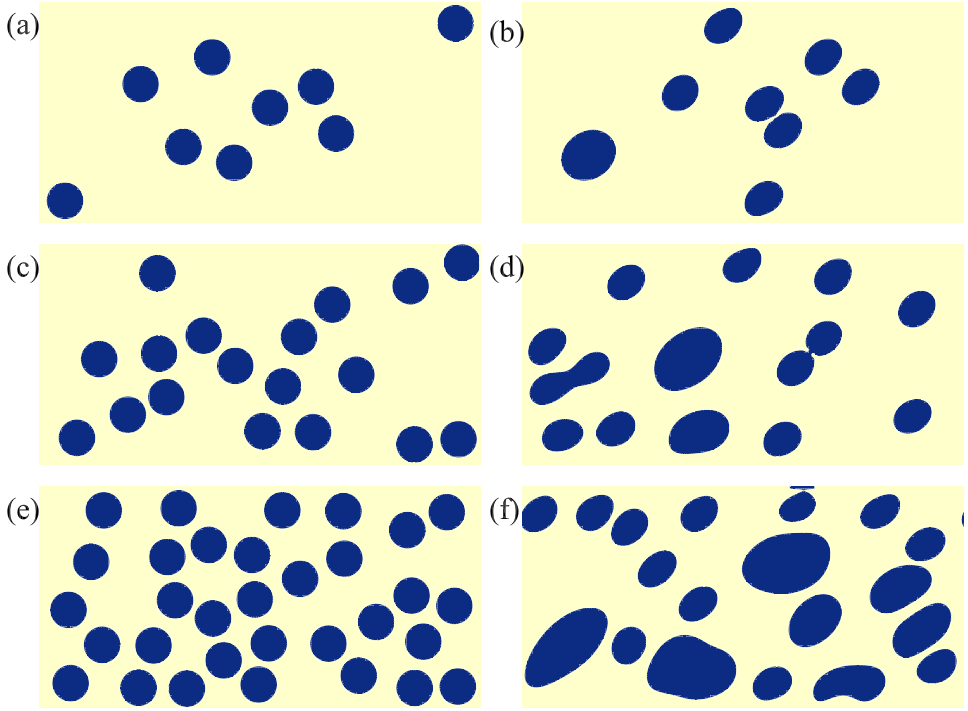

Figure 4: droplets spread randomly at fixed capillary number $Ca = 0.20$. Time progress from $t = 0$ (column left) to $t = 100$ (column right). Three volume fraction was considered, increasing from top to bottom. The portion (a-b) $\phi = 10\%$; (c-d) $\phi = 20\%$; (e-f) $\phi = 35\%$.

Similarly, in Fig. 4 we show the configuration of the droplets in random positions under simple shear, but with a fixed value of the capillary number at 0.20. The first row (Fig. 4a and 4b) correspond to the case of $\phi = 10\%$. We noticed that the deformation of the drops was more accentuated compared to the first line of Fig. 3, as we expected due to the increase in Ca. Interestingly, the number of drops in the graph is the same as in Fig. 3b. The second row shows panels

for $\phi = 20\%$. Comparing Fig. 3d with Fig. 4d it is possible to notice the influence of the increase of Ca, this second one has a greater number of drops. One of the reasons for this is that as the interfacial tension decreases, the drops tend to slide over each other, which reduces the coalescence rate as they take longer to coalesce. Ultimately, in the third row, we simulate with $\phi = 35\%$, and again we find that the coalescence has decreased compared to Fig. 3f which has higher interfacial tension

Figures 5a and 5b corresponds to the case with $\phi = 10\%$. We see that the number of drops in Fig. 5b remained the same as in the initial condition (Fig. 5a), which indicates that there was no merge of the drops. In such case, the idea that for low values of interfacial tension the drops tend not to coalesce but to slide over each other is reinforced (the number of drops for each case is found in Table 1). In addition, in the second row, Figs. 5c and 5d, we can see that is also less coalescence of the droplets compared to the previous cases of lower Ca and with the same volume fraction of the dispersed phase. Finally, Figs. 5e and 5f $\phi = 35\%$. In contrast to what we had been predicting, the number of drops decreased at the final moment (Fig. 5f) compared to the simulation of the same volumetric fraction and Ca=0.20. The merging of the droplets increases in this case, which leads us to think that there is a critical capillary number for the coalescence process.

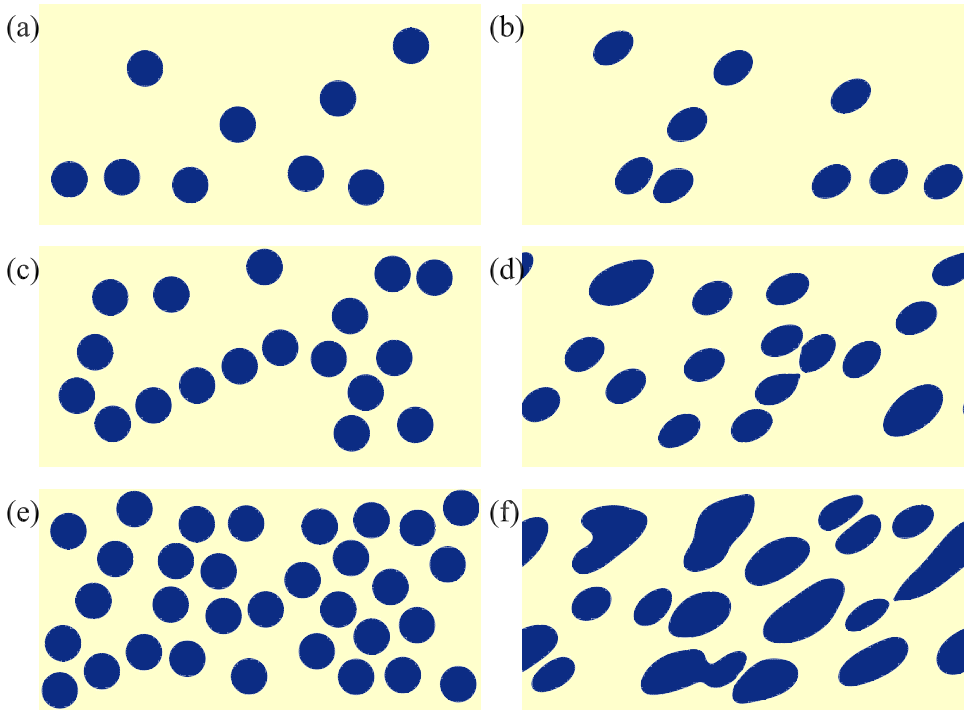

Figure 5: droplets spread randomly at fixed capillary number $Ca = 0.35$. Time progress from $t = 0$ (column left) to $t = 100$ (column right). Three volume fraction was considered, increasing from top to bottom. The portion (a-b) $\phi = 10\%$; (c-d) $\phi = 20\%$; (e-f) $\phi = 35\%$.

Hence it can be seen that droplets slide unless the capillary number is below a critical value. Shardt *et al.* (2014) performed a numerical investigation on the critical capillary number for coalescence and details of the film behavior. They found that the upper critical Ca is between 0.2020 and 0.2028, which makes sense compared to this work. For $\phi = 35\%$ from $Ca = 0.20$, we found that the coalescence decreases, as quantified by the number of drops in Tab. 1. Figure (6) shows more clearly the distinction between coalescence at low numbers of capillaries and slippage between drops with a greater Ca value than the critical capillary number due to the decrease in interfacial tension between the liquid phases.

Table 1: Number of droplets for each capillary number and volume fraction. The quantity was determined in the first iteration ($it = 0$) to the last ($it = 10^4$).

	$\phi = 10\%$		$\phi = 20\%$		$\phi = 35\%$	
	$it = 0$	$it = 10^4$	$it = 0$	$it = 10^4$	$it = 0$	$it = 10^4$
Ca=0.05	9	8	18	10	32	13
Ca=0.2	9	8	18	14	32	19
Ca=0.35	9	9	18	16	32	17

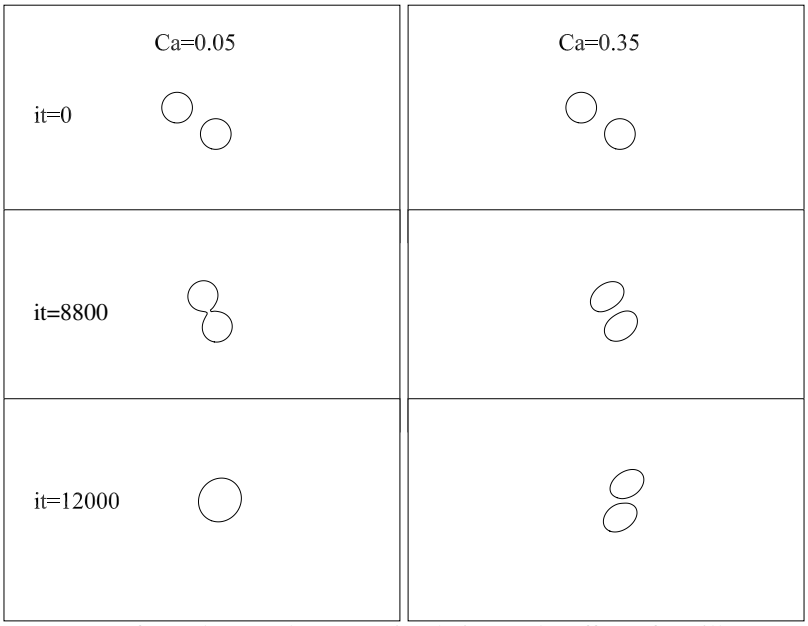

Figure 6: time sequence of two drop coalescence simulations. The effect of capillary number is shown.

5. CONCLUSIONS

In the present work, we have investigated the dynamic of monodisperse droplets spread in random positions under simple shear. A two-dimensional domain (2D) with periodic boundary conditions is imposed. The numerical methods include the level set technique to capture the droplets' interfaces and the projection method to solve the hydrodynamic problem. We simulated this system for different values of volume fraction and capillary numbers. The viscosity and density of both phases are assumed to be the same, and the Reynolds number is low enough for inertial forces to be negligible. In addition, our results in terms of deformation and orientation angle for a single droplet in simple shear agree well with the benchmark literature.

The results show that at low capillary numbers the coalescence process increases as the volume fraction of the dispersed phase increases. On the other hand, for high capillarity numbers, droplet merging decreases due to greater droplet deformation, it was observed that they tend to slide over each other for any volume fraction value. Furthermore, with these results, it is possible to verify a critical capillary number above which the phenomenon of coalescence does not occur.

Despite the good agreement, our results indicate that the coalescence rate could be higher than expected for the flow conditions, indicating that it is necessary to implement methods to avoid artificial droplet merging. For this purpose, the study presented in this work will be extended to consider the collision force model to avoid the effect of coalescence. The repulsive force can be seen as the presence of a surfactant at the interface. These models are used because diffuse interface methods are not able to predict phenomena at the microscale. Moreover, different viscosity ratios between the two fluids will be implemented to better understand the rheological behavior of concentrated emulsion. Finally, to obtain a more concentrated emulsion, a droplet growth method will be implemented. The drops start as circular and continue to grow in the Newtonian incompressible fluid, one of the changes to be made to the numerical method we use is that the velocity at the interface will have an extra diffusive term.

6. REFERENCES

Chen, D., Cardinaels, R. and Moldenaers, P., 2009. "Effect of confinement on droplet coalescence in shear flow". *Langmuir*, Vol. 25, No. 22, pp. 12885–12893.

Chen, Y. and Wang, C., 2014. "Hydrodynamic interaction of two deformable drops in confined shear flow". *Physical Review E*, Vol. 90, No. 3, p. 033010.

Cui, P. and Wang, S., 2019. "Application of microfluidic chip technology in pharmaceutical analysis: A review". *Journal of Pharmaceutical Analysis*, Vol. 9, No. 4, pp. 238–247.

De Vita, F., Rosti, M.E., Caserta, S. and Brandt, L., 2019. "On the effect of coalescence on the rheology of emulsions". *Journal of Fluid Mechanics*, Vol. 880, pp. 969–991.

Eow, J.S., Ghadiri, M., Sharif, A.O. and Williams, T.J., 2001. "Electrostatic enhancement of coalescence of water droplets in oil: a review of the current understanding". *Chemical Engineering Journal*, Vol. 84, No. 3, pp. 173–192.

Grace, H.P., 1982. "Dispersion phenomena in high viscosity immiscible fluid systems and application of static mixers as dispersion devices in such systems". *Chemical Engineering Communications*, Vol. 14, No. 3-6, pp. 225–277.

Guido, S., 2011. "Shear-induced droplet deformation: Effects of confined geometry and viscoelasticity". *Current Opinion in Colloid & Interface Science*, Vol. 16, No. 1, pp. 61–70.

Ioannou, N., Liu, H. and Zhang, Y., 2016. "Droplet dynamics in confinement". *Journal of Computational Science*, Vol. 17, pp. 463–474.

Jansen, K., Agterof, W. and Mellema, J., 2001. "Droplet breakup in concentrated emulsions". *Journal of Rheology*, Vol. 45, No. 1, pp. 227–236.

Kennedy, M.R., Pozrikidis, C. and Skalak, R., 1994. "Motion and deformation of liquid drops, and the rheology of dilute emulsions in simple shear flow". *Computers & Fluids*, Vol. 23, No. 2, pp. 251–278.

Li, W., Zhang, L., Ge, X., Xu, B., Zhang, W., Qu, L., Choi, C.H., Xu, J., Zhang, A., Lee, H. *et al.*, 2018. "Microfluidic fabrication of microparticles for biomedical applications". *Chemical Society Reviews*, Vol. 47, No. 15, pp. 5646–5683.

Loewenberg, M. and Hinch, E., 1996. "Numerical simulation of a concentrated emulsion in shear flow". *Journal of Fluid Mechanics*, Vol. 321, pp. 395–419.

Osher, S. and Sethian, J.A., 1988. "Fronts propagating with curvature-dependent speed: Algorithms based on hamilton-jacobi formulations". *Journal of Computational Physics*, Vol. 79, No. 1, pp. 12–49.

Rosti, M.E., De Vita, F. and Brandt, L., 2019. "Numerical simulations of emulsions in shear flows". *Acta Mechanica*, Vol. 230, No. 2, pp. 667–682.

Santos, T.P., Cejas, C.M. and da Cunha, R.L., 2022. "Microfluidics as a tool to assess and induce emulsion destabilization". *Soft Matter*.

Shardt, O., Derksen, J. and Mitra, S.K., 2013. "Simulations of droplet coalescence in simple shear flow". *Langmuir*, Vol. 29, No. 21, pp. 6201–6212.

Shardt, O., Mitra, S.K. and Derksen, J., 2014. "The critical conditions for coalescence in phase field simulations of colliding droplets in shear". *Langmuir*, Vol. 30, No. 48, pp. 14416–14426.

Sundararaj, U. and Macosko, C., 1995. "Drop breakup and coalescence in polymer blends: the effects of concentration and compatibilization". *Macromolecules*, Vol. 28, No. 8, pp. 2647–2657.

Sussman, M., Smereka, P. and Osher, S., 1994. "A level set approach for computing solutions to incompressible two-phase flow". *Journal of Computational Physics*, Vol. 114, No. 1, pp. 146–159.

Tadros, T., 2016. *Emulsions: Formation, Stability, Industrial Applications*. De Gruyter Textbook. De Gruyter. ISBN 9783110452242.

Taylor, G.I., 1934. "The formation of emulsions in definable fields of flow". *Proceedings of the Royal Society of London. Series A, containing papers of a mathematical and physical character*, Vol. 146, No. 858, pp. 501–523.

Vananroye, A., Van Puyvelde, P. and Moldenaers, P., 2006. "Effect of confinement on droplet breakup in sheared emulsions". *Langmuir*, Vol. 22, No. 9, pp. 3972–3974.

7. RESPONSIBILITY NOTICE

The authors are solely responsible for the printed material included in this paper.